

OPTIMISATION MULTI-OBJECTIFS EXPERIMENTALE DES LOIS DE CALAGE D'UN PROPULSEUR CYCLOIDAL MARIN

MULTI-OBJECTIVE OPTIMIZATION OF A MARINE CYCLOIDAL PROPELLER PITCH LAW USING AN EXPERIMENTAL APPROACH

G. FASSE⁽¹⁾, M. SACHER⁽²⁾, F. HAUVILLE⁽¹⁾, G. GERMAIN⁽³⁾, J.A. ASTOLFI⁽¹⁾
guillaume.fasse@ecole-navale.fr ; frederic.hauville@ecole-navale.fr

⁽¹⁾IRENav, Ecole Navale, BCRM Brest, CC600, 29240 Brest Cedex9

⁽²⁾ENSTA Bretagne, CNRS UMR 6027, IRDL, 2 rue Francois Verny, 29806 Brest Cedex9

⁽³⁾Ifremer, Hydrodynamic and Metocean Service, F-62200 Boulogne-sur-Mer

Résumé

L'étude menée porte sur le développement d'une plateforme expérimentale de grande dimension qui permet de simuler le fonctionnement d'un propulseur à axe transverse. Contrairement aux propulseurs cycloïdaux actuels utilisant un système d'entraînement des pales mécanique, la spécificité de cette plateforme est l'utilisation de servo-moteurs pour la rotation des pales sur elles-mêmes, permettant de simuler n'importe quelle loi de mouvement de pale. La gestion électrique de l'entraînement des pales utilisée dans ces travaux a nécessité le développement d'un système de contrôle-commande des moteurs afin de garantir un mouvement des pales fiable et maîtrisé. Les dimensions de la plateforme permettent l'installation d'une instrumentation variée : une mesure locale de l'effort hydrodynamique sur une pale, des capteurs d'efforts globaux sur le châssis, un couplemètre sur l'arbre principal, des capteurs de position angulaire sur chaque pale. Des procédures d'optimisation expérimentale des lois de contrôle des pales peuvent ainsi être développées dans le but d'améliorer les performances des systèmes existants. En utilisant un processus d'optimisation par méta-modèles à deux objectifs, amélioration de la poussée et du rendement, les lois optimisées permettent d'améliorer les performances hydrodynamiques des propulseurs à axe transverse. Des gains de 10 à 20 % sur le rendement et la poussée ont ainsi pu être obtenus.

Summary

The presented study deals with the development of a large experimental platform simulating transverse axis propeller. Whereas a conventional cycloidal propeller uses a mechanical system for the blade pitching, this platform employs an electrical blade-command system composed of servo-motors in order to control each blade independently. This specificity allows users to test various pitching laws to investigate cycloidal propeller performances. The platform is widely instrumented with load and torque sensors to measure instantaneous hydrodynamic forces during the rotation of the blades. Rotary encoders also measure instantaneous blade positions.

Experimental optimization, based on surrogate models (Efficient Global Optimization), is developed for the purpose of defining parameterized pitch laws which improve the performance of the existing cycloidal marine propeller. Multi-objective optimization is performed for total thrust and efficiency maximizing. Resulting optimized pitch laws increase the hydrodynamic performances of the propeller, with gains respectively from 10% to 20 % on the hydrodynamic efficiency and the thrust.

I – Introduction

Cycloidal propellers are characterized by the rotation of several blades around an axis perpendicular to the advance direction given by the rotational speed Ω and related to the azimuth angle θ ($\Omega = d\theta/dt$). Each blade is also rotating around their own axis during the main rotation of the whole system. This secondary rotation is mainly called pitch rotation, related to the blade pitch angle ϕ . This particular motion creates strong unsteady hydrodynamic forces which produces lift and drag during the main rotation. The part of hydrodynamic force in the direction of the ship advance produces the thrust force F_X whereas the part in the perpendicular direction is called side force F_Y . These propellers can easily orientate the thrust over 360° by shifting the blade pitch law over the main rotation angle.

For this type of propulsion, two kinematic modes are commonly defined according to the advance parameter λ which is the ratio of the ship advance speed V_a and the blade peripheral speed $V_r = \Omega R$, R is the propeller radius :

$$\lambda = \frac{V_a}{V_r} \quad (1)$$

Epicycloidal mode is defined for $\lambda < 1$. For this mode, rotational speed is higher than advance speed. This mode produces a high thrust and strong manoeuvrability for low advance speed (as the well-known Voith Schneider Propeller [1]). On the other hand, trochoidal mode defined for $\lambda > 1$, is used to reach higher advance speed but with a lack of efficiency during starting phases. For epicycloidal mode, the blade chord is roughly following the tangent of the main rotation, whereas for trochoidal mode the blade oscillates around the advance direction [2].

As an interesting marine propulsion system, cycloidal propeller have been studied by the IRENav with the developpment of a blade-controlled plateform [3]. Thanks to an electrical blade-command design, this platform allows to reproduce blades' kinematic from all conceivable movements (trochoidal or epicycloidal kinematics). This electrical blade-command also allows authors to perform pitch law optimization to improve performances of current cycloidal propellers. The aim of this article is to present an experimental optimization using a Gaussian process based method, coded by Sacher [4], to maximize

both thrust and efficiency of cycloidal propellers. The optimization uses experimental measurements collected from the instrumented blade-controlled platform. Experiments are performed at the Ifremer current tank. These experimental facilities are described in the first section as well as the parameterization of the pitch laws and the optimization method. The second section deals with the results of sinusoidal laws which represent classical pitch laws for current propellers [5]. These results are compared to the optimization for $\lambda=1.2$ simultaneously from thrust and efficiency aspects.

II – Method and optimization problem

II – 1 Experimental platform

To perform the optimization, the experimental blade-controlled platform, called SHIVA, is operating at the Ifremer wave and current flume tank. Figure 1 gives an overview of the platform and its positioning at the flume tank. The system is composed of a triangular frame [F] in which three blades [I] are mounted. These blades are rotating thanks to three servo-motors [E] that gives them independent motions. The outer frame [D] allows the platform to be elevated above the tank in order to dive just the blades under the water line. The design of the platform allows users to change the rotor diameter from 0.4 m to 0.8 m. The blade number N is fixed at 3. Each blade has a chord length $c = 0.35$ m and a span $l = 1$ m with a blade cross section of NACA 0018, with a diameter fixed at $D = 0.8$ m. These dimensions lead to a solidity of the propeller $\sigma = 2.62$ ($\sigma = \frac{2Nc}{D}$).

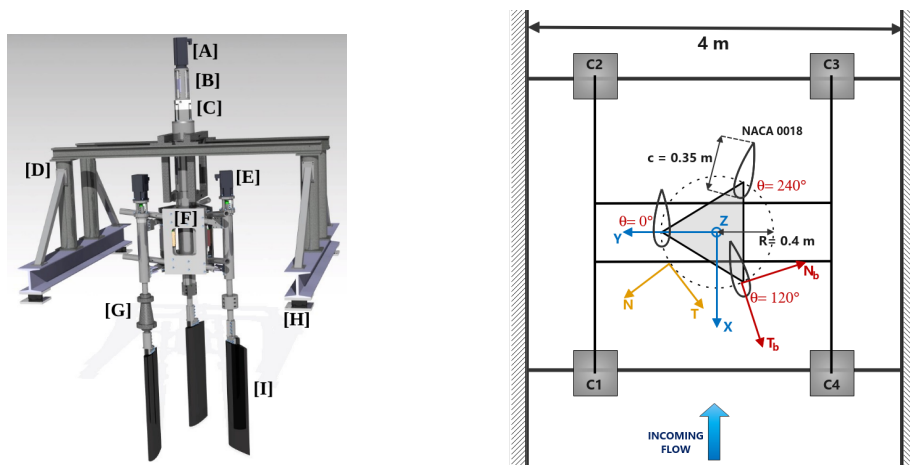


FIGURE 1 – Blade-controlled platform and its positioning at the current flume tank

The particularity of this experimental platform lies on the electric blade pitch command. The triangular frame is driven by the 2.5kW main motor [A] located at the top of the platform. A 50-ratio speed reducer [C] is used to increase the torque and fit the rotational speed for our experiment values (~ 0 -50 RPM). Each blade is independently actuated by a 0.8kW auxiliary motor [E]. The blades rotate around the quarter of their chord, close to the aerodynamic center for the NACA 0018. This rotation is called blade pitch and is referred to as the oriented angle φ between the tank flow direction (X-axis) and the blade chord. The pitch angle can also be defined as the oriented angle β between the ortho-radial line of the main rotation and the blade chord. These two pitch angles are linked by the relation $\theta = \varphi - \beta$. The azimuth position of a blade θ is the position of its chord quarter on the main rotation disk, and for an arbitrary time Δt , $\theta = \Omega \Delta t$ where Ω is the main rotational speed.

Expression of the pitch angle in function of the azimuth position is the pitch law. These laws are tabulated as discrete functions on an embedded micro-controller unit which send regulation orders directly to the speed controllers for each blades in order to follow the reference pitch law.

In addition, SHIVA is widely instrumented to measure time-dependant hydrodynamic loads and blade angular positions. Rotary incremental encoders are used simultaneously for the control loop as feedback and for loads measurements as projection angle. The azimuth position is also recorded by a rotary incremental encoders with a precision of 0.014° .

One blade is instrumented with an embedded 5-components load-cell [G] which measure local hydrodynamic loads in the direction of the blade's chord \mathbf{T}_b (measuring range of 200 N) and normal to the blade \mathbf{N}_b (measuring range of 900 N). This load-cell also measures the torque \mathbf{C}_b applied on the blade by hydrodynamic loads (measuring range of 60 Nm). Four fixed 3-components load-cell [H] located between the outer frame I-beams and the tank I-beams provide global solicitations of the propeller in the X,Y and Z directions (measuring range of 5000 N in the X and Y direction and 7000 N for the Z direction). At least, a torque sensor [B] is installed between the main motor and the speed reducer and measures the torque applied on the main driveshaft \mathbf{C}_{tot} (measuring range of 20 Nm). Due to the wider measuring range of these fixed load-cell, in comparison with the embedded load-cell, post-processing of the loads is done with local hydrodynamic loads (for more precision, refer to [3]). The embedded load-cell measures temporal voltages which are highly disturbed by high frequencies of electromagnetic environment mainly due to the Pulse Width Modulation of speed controllers. Low-pass filter (35Hz cut-frequency) is thus applied on temporal signals. Then voltages are converted into loads thanks to the transfer matrix determined by calibration. Finally, thanks to the acquisition of angular positions, forces in blade reference frame (\mathbf{F}_{N_b} , \mathbf{F}_{T_b}) are projected into rotor reference frame (\mathbf{F}_N , \mathbf{F}_T) and absolute reference frame (\mathbf{F}_X , \mathbf{F}_Y) by equations (2) and (3).

$$\begin{pmatrix} F_T \\ F_N \end{pmatrix} = \begin{pmatrix} \cos(\beta) & -\sin(\beta) \\ -\sin(\beta) & -\cos(\beta) \end{pmatrix} \begin{pmatrix} F_{T_b} \\ F_{N_b} \end{pmatrix} \quad (2)$$

$$\begin{pmatrix} F_X \\ F_Y \end{pmatrix} = \begin{pmatrix} \cos(\theta) & \sin(\theta) \\ -\sin(\theta) & \cos(\theta) \end{pmatrix} \begin{pmatrix} F_T \\ F_N \end{pmatrix} \quad (3)$$

Then instantaneous forces are phase-averaged over at least 30 revolutions to one period, shifted of $\frac{\pi}{3}$ and $\frac{2\pi}{3}$, and summed to give the total force acting on the three blades. Lastly, total thrust coefficient, torque coefficient and hydrodynamic efficiency are calculated as the non-dimensional averaged values :

$$C_{F_X} = \frac{\overline{F_{X_{tot}}}}{0.5\rho S V^2} \quad C_T = \frac{\overline{C_{tot}}}{0.5\rho S D V^2} \quad \eta = \frac{\overline{F_{X_{tot}}} V}{\overline{C_{tot}} \Omega} \quad (4)$$

Where $\overline{F_{X_{tot}}}$ and $\overline{C_{tot}}$ are respectively the mean of total thrust and total torque (measured on the main torque sensor) over 360° , S is the swept frontal area ($S = Dl$) and V the flume tank flow velocity. These experimental performances are measured and spent through the optimization code to evaluate the objective function. To perform the optimization, the choice of the parameters have to be suited for maximizing the performance of cycloidal propeller. The blade motion is directly linked to the hydrodynamic force generation.

II – 2 Parametric model

The method presented in this paper consists in defining the pitch law by a spline passing through four control points which are given by 3 parameters. Figure 2 illustrates the parameterization for two random laws.

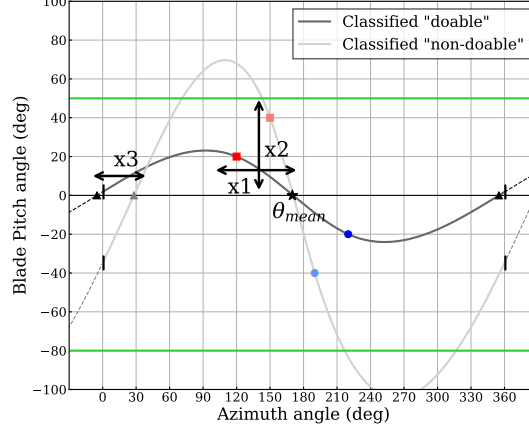


FIGURE 2 – At the left, pitch law parameterization method. At the right, classification iso-surface of "doable" pitch law in the parametric space.

The four control points are the first black triangle, the red square, the blue circle and the last black triangle. These points are defined with three parameters :

1. \mathbf{x}_1 gives the abscissa of the two central points (red square and blue circle) by setting the distance of this abscissa and the central position θ_{mean} :

$$\begin{aligned} x_{red\ square} &= \theta_{mean} - \mathbf{x}_1 \\ x_{blue\ circle} &= \theta_{mean} + \mathbf{x}_1 \end{aligned}$$

2. \mathbf{x}_2 give the ordinate of these two central points :

$$y_{red\ square} = \mathbf{x}_2 \quad ; \quad y_{blue\ circle} = -\mathbf{x}_2$$

3. \mathbf{x}_3 allows an offset of the law for the zero crossing at the beginning and the end of the spline (the last black triangle is the 2π -offset of the first one).

$$x_{black\ triangle} = \mathbf{x}_3 \bmod 360 \quad ; \quad y_{black\ triangle} = 0$$

For the presented results, the central position θ_{mean} is set at 170 degrees. This position involves a non-symmetrical pitch law which is the intent of this optimization as explained in the context. The non-symmetrical construction of the law also implies a different gradient between the start ($\theta=0^\circ$) and the end of the spline ($\theta=360^\circ$). To fix this problem, the spline is defined on 10 periods (5 before and 5 after) to ensure the continuity at $\theta=0^\circ$ and $\theta=360^\circ$ (with an error of 10^{-7}).

Each parameter can move through the following ranges :

$$\Delta x_1 = [0.5 : 120]; \quad \Delta x_2 = [0.5 : 80]; \quad \Delta x_3 = [-5 : 40]$$

This method of parameterization implies a weakness which occurs when two points of the spline are to close, the amplitude of the spline can be very high. To avoid this, a classification is used and taking into account during the optimization procedure. This

classification consists on defining two limits (high and low) to the spline and classify the parameterized spline "doable" if all the points of the spline are between these two limits. These limits are represented in green on the left of the Figure 2 and fixed at $\varphi = 50^\circ$ and $\varphi = -80^\circ$ for the present experiments. These limits have been chosen after experiments considerations : high amplitude laws imply an acceleration for auxiliary motor which is too high and in the half downstream it has been sensed that the pitch must be higher than the upstream to give the ability of the blade to "cut" the wake.

For hundred arbitrary laws have been generated over the range of the 3 parameters to estimate the classification model. The right sub-figure of Figure 2 represents this classification model with the iso-surface of 50%-probability of the law to be "doable". This figure shows in the front the area of laws which are considered "doable" and in the back those which have high probability to be "non-doable". During the optimization process, the classification is taken into account and so the area of interest for the new optimized point is always located inside the front area of 50%-probability to be "doable".

II – 3 Multi-objective Surrogate-based Optimization

We consider abstract optimization problems, where several objectives have to be minimized simultaneously over a design variable $\Omega \subset \mathbb{R}^d$:

$$\min_{\mathbf{x} \in \Omega} f_1(\mathbf{x}), \dots, f_m(\mathbf{x}) \quad \text{s.t.} \quad \mathbf{g}(\mathbf{x}) \leq 0 \quad (5)$$

where $\mathbf{x} = (x_i)_{1 \leq i \leq d}$ is a vector of design variables, $\mathbf{f} = (f_j)_{1 \leq j \leq m}$ is a vector of objective functions to be minimized ($f_i : \Omega \mapsto \mathbb{R}$), and $\mathbf{g} = (g_k)_{1 \leq k \leq p}$ is a vector of inequality constraints ($g_k : \Omega \mapsto \mathbb{R}$). The existence of an optimal solution, minimizing all objectives at once is usually not granted. This leads to the search for an optimal set of solutions, called the Pareto front.

Surrogate-based optimization methods rely on the sequential construction of statistical surrogate models, using training sets of computed objective and constraint function values, that are refined according to a prescribed infilling strategy (i.e. merit functions [6]). At each iteration of the iterative surrogate-based optimization, a new design vector \mathbf{x}_{n+1} is thus added to \mathcal{X} , and finally \mathbf{f} and \mathbf{g} are computed. A new iteration can then start by updating surrogate models, and the iterative process is repeated until a stopping criterion is satisfied or the resources allocated to the optimization have been exhausted.

In this work, a probabilistic classification model is built using the union of doable and non-doable training sets. The classifier is then incorporated in the surrogate-based optimization procedure to avoid proposing new design vectors in the non-doable domain while improving the classification uncertainty if needed. Thus, two new design vectors are determined under the constraint to be in the doable domain and added to \mathcal{X} at each new iteration of the iterative surrogate-based optimization. Specifically, two criteria are considered to allow respectively the improvement of the computed Pareto front (Expected Improvement Matrix Hypervolume criterion) and the search of the best compromise in this Pareto Front (Median Compromise of the Pareto Front). This latter criterion consists in selecting the median trade-off by considering the rank, from the Pareto set, of each objective function prediction. This definition allows a design vector compromise to be determined without the need for weights or scaling of objective function.

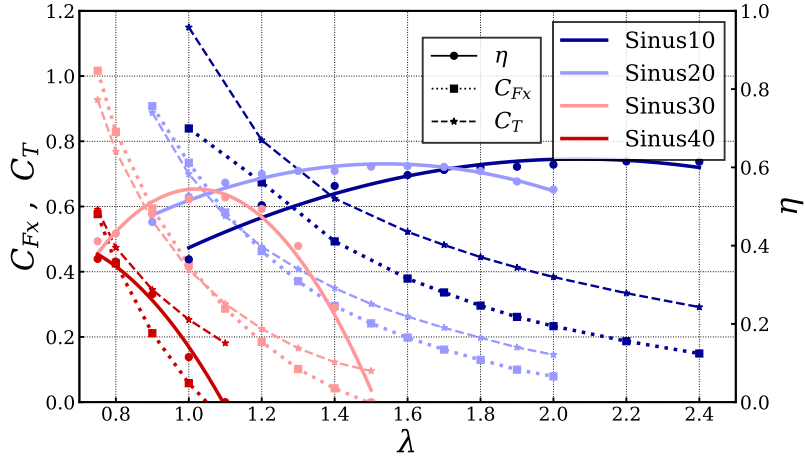


FIGURE 3 – Global performances (thrust and torque coefficients at the left scale for colored dotted lines with square and star markers and efficiency at the right scale for colored lines with circle markers) for four amplitudes of sinusoidal laws, differentiated by the color.

III – Experimental measurements and optimization results

First experiments are undertaken at the Ifremer flume tank for sinusoidal pitching laws with the SHIVA platform. The measurements have been done for various advance parameter values to evaluate the performances of the cycloidal propeller over a range of operating conditions. Then the optimization procedure is carried out for $\lambda=1.2$.

III – 1 Sinusoidal pitch results

All the results with sinusoidal laws are measured with a tank speed V fixed at 0.8 m/s, corresponding to a global Reynolds number $Re = \frac{VD}{\nu}=640\ 000$. The rotational speed Ω is then adjust to the desired λ value.

Measurements are registered on 30 rotations of the platform after waiting that the flow is well established. Blade-control parameters are adjusted in function of the rotational speed to ensure a pitch track with a maximal error under 1 degree. Signals from the instrumentation are converted in force and projected to calculate the thrust force and main torque. These signals are then phase-averaged over the 30 periods and non-dimensionalized according equations 4. More details of the signals treatment for these experiments is providing by Fasse [7].

Results, presented in Figure 3, reveal that depending on the value of the advance parameter, the maximal efficiency is reached at different values of λ for each pitch law. This first conclusion corroborates the benefit of an adaptable pitch system to adjust the pitch to the desired operating mode. It also means that during the acceleration phase, it is preferable to start with high amplitude pitch law then decrease the pitch amplitude. However, the results for the Sinus40 law show that for $\lambda < 1$, a trochoidal law is not well-suited for the epicycloidal mode. The transition between epicycloidal and trochoidal mode is complex in term of pitch law shape and requires a specific investigation that is not detailed in this paper. Furthermore, because motors of the platform have encountered some limitations in epicycloidal, the study presented here is focused on the trochoidal mode.

Concerning the thrust, the Sinus10 law has the higher values for all the advance parameters. It shows that for manoeuvre which requires high thrust, the pitch amplitude must be decreased, balancing a reduction of the efficiency. But the efficiency hardly falls for λ close to 1 because the required torque to rotate the propeller is rising.

Sinusoidal pitch law are suited for mechanic pitch systems as periodic and symmetrical blade motion. But there is no reason why the pitch law definition should be symmetrical. Indeed, the complexity of the flow through cross-flow propellers implies a strong discrepancy between upstream and downstream halves. It is why an experimental optimization is proceeded with a relevant parameterization of the pitch law.

III – 2 Optimized pitch results

Experimental conditions for the optimization are as follows : $\lambda=1.2$, tank speed $V=0.8$ m/s, SHIVA rotational speed $\Omega=15.92$ RPM. Before tackle the optimization, a sampling of 35 pitch laws is carried out through the parametric space using Latin Hypercube Sampling method [8]. Then approximately 50 optimization steps have been performed during 8 hours of experiments (approximately 10 minutes by step). One step of optimization consists on :

1. Generate the pitch law with the three parameters (x_1, x_2, x_3) .
2. Upload the pitch law on the SHIVA platform and start the measurement of force signals after waiting few minutes that the flow is well established.
3. After a duration corresponding to 30 rotations of SHIVA, measurements are post-treated to calculate the value of objective function (here is the mean thrust coefficient C_{Fx} and the efficiency η)
4. These new data are computed to update the two meta-models of thrust and efficiency and the Pareto Front.
5. The optimizer gives back two new triplet of parameters after computing the EIMH and the MCPF criterion to respectively search for the best improvement for both objectives and search for the best compromise on the Pareto Front.
6. Return to the stage one.

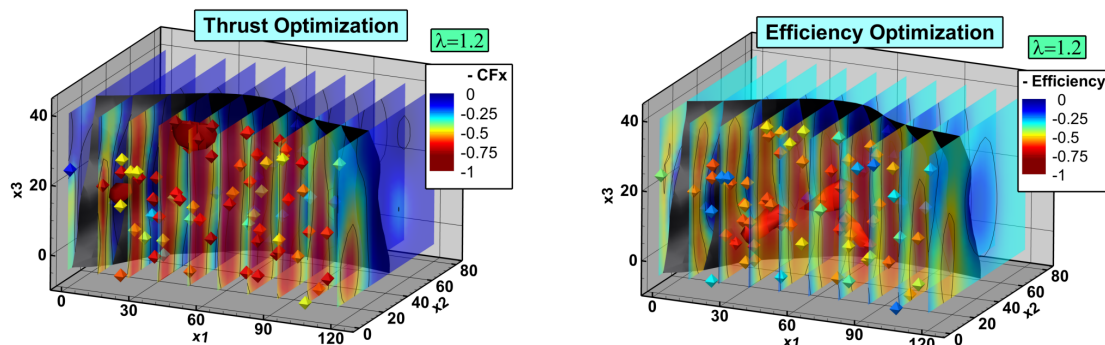


FIGURE 4 – Meta-models for thrust (left) and efficiency (right) at the end of multi-objective optimization.

Figure 4 gives the two meta-models in the 3d parametric space obtained at the end of the optimization process. Octahedrons are the experimental points located in function of the parameters which were used to generated the pitch law. As mentioned earlier, all experimental points are inside the front area delimited by the black 50%-probability iso-surface. Octahedrons are colored with their objective value (total thrust coefficient at the

left and efficiency at the right). Slices show the meta-model inferred from experimental points and so colored in function of the objective value. For respectively the thrust and the efficiency, the red iso-surface represents the pockets of the meta-model for which the thrust coefficient is higher than 0.75 (absolute value) and respectively higher than 0.63 for the efficiency. Because the optimizer uses a minimization procedure during the optimization, objective function are given with negative sign.

These results show that the pocket of maximal thrust is not located in the same area than the one obtained for the efficiency. It proves that for $\lambda=1.2$, the blade motion which produces the maximal thrust is not this which is the best efficient. The law which maximize the thrust is generated by the triplet (48.88, 7.37, 39.19) whereas this which maximize the efficiency is given by the triplet (37.07, 17.92, 8.93). According to the value of parameter x_2 , which deals with the amplitude of the law, optimization shows that the law with the best efficiency has an amplitude around 20° whereas for thrust maximizing the amplitude of the law is lower. This result confirms observations about sinusoidal laws for which Sinus20 have a better efficiency at $\lambda=1.2$ than Sinus10 but a lower thrust coefficient (see Figure 3).

These two meta-models reveal that there is a compromise between thrust maximization and hydrodynamic efficiency. The Median Compromise of the Pareto Front criterion, which is based on ranking trade-off between multiple objectives, permits to search for the best law satisfying both objectives without regarding objective values but only the rank of each objective through all measured laws. The best compromise is the law for which the sum of the rank is minimum. Thus no weighting of objectives is necessary.

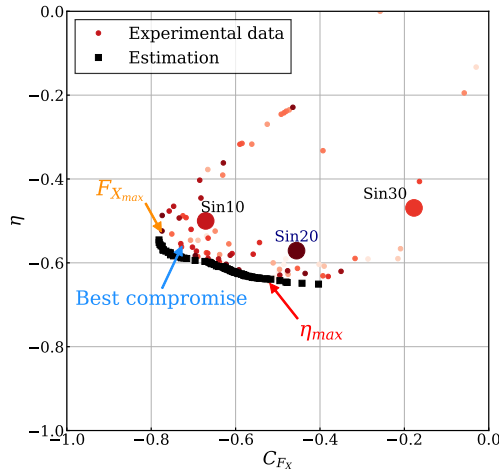


FIGURE 5 – Pareto front obtained from experimental optimization and compared to sinusoidal pitch results.

Figure 5 presents the Pareto Front obtained from the experimental optimization. The little colored circles correspond to each generated laws and are plotted in function of the experimental results in thrust coefficient and efficiency pairs. Black squares correspond to a virtual front estimated by the optimizer based on the experimental results. Finally, sinusoidal results for $\lambda=1.2$ are displayed to compare performances.

As expected, there are significant performance benefits to be gained with optimized law for both objectives. The efficiency gain is around **8%** between Sinus20 and the Pareto Front ($\eta_{Sinus20} = 0.57$ and $\eta_{Optim} = 0.64$) while the advantage in thrust is over **11%** between Sinus10 and the Pareto Front ($CF_{X_{Sinus10}} = 0.67$ and $CF_{X_{Optim}} = 0.78$).

Figure 6 gives general results (pitch law φ and blade forces F_X and F_Y) for the 20-

sinusoidal law (in dark blue) and three optimized laws : with the best thrust (in orange), the best efficiency (in red) and the best compromise (in light blue). The right sub-figure shows the experimental measurement of hydrodynamic forces along θ positions (each 30°). These three laws are also represented in the Figure 5 as well as the Sinus20 law.

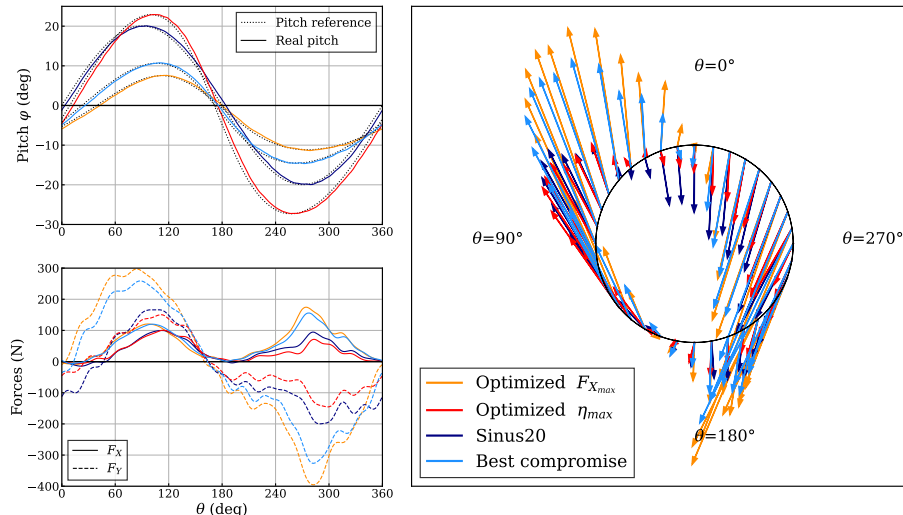


FIGURE 6 – Detailed results of hydrodynamic forces generated by three different laws (Sinus20, Optimized law maximizing the trust $F_{X_{max}}$ and Optimized law maximizing the efficiency η_{max}) over azimuth positions.

Concerning the pitch law, optimization procedures reveal two main differences with sinusoidal laws :

- Non-zero pitch at $\theta=0^\circ$ (dephasing effect)
- Higher pitch for downstream positions than for upstream positions (non-symmetrical effect)

The first effect is due to the x_3 parameter which forces the law to cross the $\varphi=0$ -line at $\theta=x_3$ ($\theta=39.19^\circ$ for the thrust maximization law and $\theta=8.93^\circ$ for the efficiency maximization law). While sinusoidal law passes through the point $(\theta=0, \varphi=0)$, optimized laws have slight incidence at $\theta=0^\circ$. This leads to a reduction of the hydrodynamic forces near $\theta=0^\circ$ especially side force component F_Y . For these positions, thrust force is close to zero, so the reduction of side force have a favorable effect on the efficiency. Indeed, by decreasing the hydrodynamic loads at these positions the total torque required to turn the whole platform is also reducing.

The non-symmetrical effect has two different impacts regarding the optimized laws. For the $F_{X_{max}}$ law, the thrust peak in the upstream is shifted towards $\theta=90^\circ$ (whereas the peak is reached near $\theta=120^\circ$ for the two other laws). In the downstream half, the thrust peak is even higher than the upstream half, contrary to the η_{max} and the Sinus20 laws for which the downstream thrust is lower than in upstream. But the thrust increasing comes with a side-force inflation which induces a diminution of efficiency. For the η_{max} law, the non-symmetrical effect leads to significant decrease the side-force F_Y in the downstream half in comparison with the Sinus20 and other optimized law, while thrust force is quite similar to the Sinus20 law. And so the required torque to the main rotation is lower than the classic sinusoidal law which implies a better efficiency. Finally the law which have the best compromise between thrust and efficiency has a pitch shape located between $F_{X_{max}}$ law and η_{max} law. Concerning the thrust, this law is similar to the $F_{X_{max}}$ law in

the upstream and almost for the downstream. But the significant gain is on the side-force which is clearly lower than for the $F_{X_{max}}$ law, resulting to a better efficiency.

This trade-off between efficiency and thrust can be modified into the search of the law giving the best efficiency for a given value of thrust. Indeed, for propulsion purpose, the idea is to reach a desired advance speed while overcoming the hull resistance. So knowing this hull resistance, which depends on the hull shape, dimensions and the advance speed, this procedure is very interesting for the design of vertical axis propeller.

To go further, a generalization of this optimization for different λ values ensures an optimal law for a wide range of velocities and operation modes.

IV – Conclusion and Perspectives

This paper presented an experimental optimization procedure of a cycloidal propeller blade pitch laws. Indeed, for this specific type of propulsion, characterized by the rotation of blades around an axis perpendicular to the ship advance speed, the blade motion has a huge impact on the propeller performances.

By using a suitable parameterization of the pitch laws allowing a wide diversity of pitch motion, the multi-objective optimization can be performed with the full electric SHIVA platform. Both thrust and efficiency maximization are chased to satisfy two different objectives. Results shows that a trade-off is necessary concerning the pitch law shape to maximize the thrust or the efficiency. A Pareto Front is thus determined between these two objectives to search for the best compromise law. The results show a significant improvement of both thrust and efficiency for the best compromise. Gains respectively from 10% to 20% on the hydrodynamic efficiency and the thrust are obtained with optimized laws.

Finally, because experimental optimization takes time, the procedure have been carried out for only one λ value. As perspectives, it will be interesting to repeat this optimization for a range of λ values to compare the performances of the cycloidal propeller for many operating points. An upgrade the SHIVA platform with the installation of a Artificial Intelligence can lead to the automatization of the optimization process.

Références

- [1] E. Schneider, Blade Wheel, US Patent 168150, URL : <https://patents.google.com/patent/US1681500>, 1928.
- [2] N. Bose, P.SK. Lai, Experimental performance of a trochoidal propeller with high-aspect-ratio blades, Marine Technology and SNAME News, 26 (3) 192–201, 1989.
- [3] G. Fasse, F. Becker, F. Hauville, J.A. Astolfi, G. Germain, An experimental blade-controlled platform for the design of smart cross-flow propeller, Ocean Engineering, Elsevier, vol. 250, 110921, 2022.
- [4] M. Sacher, F. Hauville, R. Duvigneau, O. Le Maitre, N. Aubin, M. Durand, Efficient optimization procedure in non-linear fluid-structure interaction problem : Application to mainsail trimming in upwind conditions, Journal of Fluids and Structures, 69 209–231, 2017.
- [5] B.T. Roesler, M.L. Kawamura, E. Miller, M. Wilson, J. Brink-Roby, E. Clemmenson, M. Keller, B.P. Epps, Experimental performance of a novel trochoidal propeller, Journal of Ship Research, 60 (1) 48–60, 2016.

- [6] V. Picheny, T. Wagner, D. Ginsbourger, A benchmark of kriging-based infill criteria for noisy optimization, *Structural and Multidisciplinary Optimization*, 48 (3) 607–626, 2013.
- [7] G. Fasse, Développement d'une plateforme expérimentale simulant le fonctionnement d'un propulseur à axe transverse à pales commandées, Thèse de doctorat, 2022.
- [8] M.D. McKay, R.J. Beckman, W.J. Conover, A comparison of three methods for selecting values of input variables in the analysis of output from a computer code, *Technometrics*, 42 (1) 55–61, 2000.